RSC Advances

PAPER

View Article Online
View Journal | View Issue

Cite this: *RSC Adv.*, 2016, **6**, 34849

Thiophene-*S*,*S*-dioxidized indophenine (IDTO) based donor–acceptor polymers for n-channel organic thin film transistors†

Yunfeng Deng, Jesse Quinn, Bin Sun, Yinghui He, Jackson Ellard and Yuning Li*

Received 3rd February 2016
Accepted 29th March 2016

DOI: 10.1039/c6ra03221d

www.rsc.org/advances

Two donor–acceptor (D–A) conjugated polymers, **PIDTOBT** and **PIDTOBTz**, based on thiophene-*S*,*S*-dioxidized indophenine (IDTO) as the acceptor building block are synthesized for solution processed organic thin-film transistors (OTFTs). The influences of the donor unit on the photophysical, electrochemical and electron-transport properties were investigated. These polymers possess very deep highest-occupied molecular orbital (HOMO) and lowest unoccupied molecular orbital (LUMO) energy levels due to the strong electron accepting capability of the IDTO moiety. In OTFT devices, both polymers exhibited unipolar n-type charge transport characteristics with electron mobility up to 0.18 $cm^2 V^{-1} s^{-1}$.

Introduction

The development of new p-type (hole-transporting), n-type (electron-transporting), and ambipolar (hole- and electron-transporting) polymer semiconductors for organic thin film transistors (OTFTs) has been a focus area of printed electronics due to their tunable optoelectronic properties and ability to enable low cost, mechanical flexible and large-area devices.[1–4] To date, some p-type polymers with hole mobility over 10 $cm^2 V^{-1} s^{-1}$ have been reported.[5–7] In contrast, the development of unipolar n-type polymers lags behind.[8,9] For a number of applications such as complementary metal-oxide-semiconductor (CMOS)-like logic circuits, all-polymer heterojunction photovoltaics and organic light-emitting diodes, both p-type and n-type polymers are required.[10–13] Hence the development of high performance unipolar n-type polymeric semiconductors has drawn increasing attention recently.[9,14–17]

The key factor for achieving n-type charge transport performance of a polymer semiconductor is to obtain low HOMO (highest occupied molecular orbital) and LUMO (lowest unoccupied molecular orbital) energy levels, which could suppress the hole injection and facilitate the electron injection, respectively.[12,18,19] In recent years, the construction of donor–acceptor (D–A) polymers has proven to be one of the most effective strategies to obtain high performance n-type polymer semiconductors because the intermolecular interaction strengthened by the D–A interaction shortens the π–π distance for efficient charge hopping.[1,17,20,21] Compared with a large library of electron donor building blocks, the electron acceptor building blocks suitable for constructing n-type D–A polymer semiconductors are still limited. Therefore, new electron acceptor building blocks need to be explored in order to develop high performance n-type polymer semiconductors.[22–24] Ideally, the electron acceptor building blocks should be easy to synthesize and strongly electron-withdrawing to adequately decrease the HOMO and LUMO energy levels of the resulting D–A polymers.

Recently, we have developed a new electron acceptor building block, the (*E*,*E*,*E*)-form thiophene-*S*,*S*-dioxidized indophenine (IDTO) by oxidation of the well-known blue dyestuff, indophenine, to construct D–A polymers that show unipolar n-type performance with an electron mobility over 0.1 $cm^2 V^{-1} s^{-1}$.[25] Compared with other electron acceptor building blocks, IDTO has the following four advantages: (1) deep frontier orbital energy levels (Fig. S5†), which can effectively reduce the HOMO and LUMO energy levels of the polymers;[26] (2) rigid and coplanar π-backbone, which could promote intermolecular π–π overlap for efficient charge transport;[27,28] (3) possessing a quinoidal form structure, which would be more beneficial for efficient charge conduction along the polymer backbone than the aromatic form;[29–31] (4) the ease of synthesis from inexpensive starting materials, isatin and thiophene. To further explore the potential of this new electron acceptor building block, in this work we report two new D–A polymers based on IDTO as the electron acceptor moiety, **PIDTOBT** and **PIDTOBTz**, where 2,2′-bithiophene (BT) and 2,2′-bithiazole (BTz) serve as the electron donating moieties, respectively, in order to improve the molecular ordering and thus the carrier mobility. BT[32–35] and BTz[36–39] have been frequently used for constructing high performance polymer semiconductors for OTFTs because of their ability to achieve high coplanarity of the

Department of Chemical Engineering, Waterloo Institute for Nanotechnology (WIN), University of Waterloo, 200 University Ave W, Waterloo, Ontario, N2L 3G1, Canada. E-mail: yuning.li@uwaterloo.ca; Fax: +1-519-888-4347; Tel: +1-519-888-4567 ext. 31105

† Electronic supplementary information (ESI) available. See DOI: 10.1039/c6ra03221d

polymer backbone and fine-tune the energy levels of the resulting polymers. To our delight, **PIDTOBT** exhibited high electron mobilities up to 0.18 $cm^2 V^{-1} s^{-1}$ in OTFTs. On the other hand, **PIDTOBTz** showed much lower electron mobilities of up to 0.017 $cm^2 V^{-1} s^{-1}$ due to its amorphous film and low molecular weight.

Experimental section

Materials and characterization

All starting materials were purchased from commercial sources and used without further purification. (3*E*,3′*E*)-3,3′-((*E*)-1,1,1′,1′-Tetraoxido-5*H*,5′*H*-[2,2′-bithiophenylidene]-5,5′-diylidene)bis(6-bromo-1-(4-octadecyldocosyl)indolin-2-one) (**IDTO-40**)[25] and 5,5′-bis(trimethylstannyl)-2,2′-bithiazole[40] were synthesized according to the reported methods. Computational simulations were performed using density function theory (DFT) calculation with the 6-311G+(d, p) basis set and all the orbital pictures were obtained using Gauss View 5.0 software. GPC measurements were performed on Malvern HT-GPC at 140 °C using 1,2,4-trichlorobenzene as eluent and polystyrene as standards. The polymer solutions were pre-dissolved at 170 °C for at least 2 h. ^{1}H-NMR data were recorded with a Bruker DPX 300 MHz spectrometer. The chemical shifts of ^{1}H-NMR was referenced to tetramethylsilane (TMS, 0 ppm). Thermal gravimetric analyses (TGA) were carried out on a TA Instruments SDT 2960 with scan rate of 10 °C min^{-1} under nitrogen. UV-Vis-NIR spectra were recorded on a Thermo Scientific Genesys 10 UV instrument using polymer solutions in 1,1,2,2-tetrachloroethane (TCE) and polymer films spin-coated onto quartz substrates. Cyclic voltammetry (CV) data were obtained on a CHI600E electrochemical analyser in dry acetonitrile containing 0.1 M n-Bu_4NPF_6 as an electrolyte under nitrogen at a scan rate of 100 mV s^{-1}. An Ag/AgCl reference electrode and two Pt disk electrodes as the working and counter electrodes were used. Ferrocene was used as the reference, which has a HOMO energy value of −4.8 eV. A Bruker D8 Advance powder Diffractometer with standard Bragg–Brentano geometry was used to collect the XRD patterns of polymer thin films using Cu K_α radiation ($\lambda = 1.5406$ Å), then the same samples were used to record atomic force microscopic (AFM) images with a Dimension 3100 scanning probe microscope. Elemental analysis was performed on a VarioEL elemental analysis system.

Fabrication and characterization of OTFT devices

The bottom-contact, bottom-gate configuration was used for all OTFT devices, which were fabricated on a heavily n-doped Si/SiO_2 substrate. The thermally grown SiO_2 layer is ~300 nm thick. The gold source/drain pairs were obtained by conventional photolithography and thermal deposition to give a defined channel length (30 μm) and channel width (1000 μm). The Si/SiO_2 substrate was treated with air plasma, followed by cleaning with acetone and isopropanol in an ultra-sonic bath. Subsequently, the substrate was modified with dodecyltrichlorosilane (DDTS) (1% in toluene) at room temperature for 20 min. Then a polymer solution in TCE (**PIDTOBT**) or chloroform (**PIDTOBTz**) was spin-coated onto the substrate at 3000 rpm for 60 s to give a polymer film (~40 nm). After thermal annealing at given temperatures in a glove box for 20 min, the devices were characterized in the same glove box with an Agilent B2912A Precision Source/Measure Unit. The hole and electron mobilities are calculated in the saturation regions according to the following equation:

$$I_D = \frac{W}{2L} C_i \mu (V_G - V_T)^2$$

where I_D is the drain current, W and L are the device channel width and length, C_i is the gate dielectric layer capacitance per unit area (~11.6 nF cm^{-2}), μ is the carries mobility, V_G and V_T are gate voltage and threshold voltage.

Synthetic procedures

Synthesis of PIDTOBT. To a 25 mL dry Schlenk flask was added **IDTO-40** (100 mg, 0.056 mmol), 5,5′-bis(trimethylstannyl)-2,2′-bithiophene (28.34 mg, 0.057 mmol) and tri(*o*-tolyl)phosphine (1.36 mg, 8 mol%). After degassing and refilling argon for 3 times, a solution of tris(dibenzylideneacetone)-dipalladium (1.03 mg, 2 mol%) in dry chlorobenzene (4 mL) was added under an argon atmosphere. The flask was sealed and stirred at 130 °C for 48 h. Four drops of bromobenzene was added and the reaction was kept at 130 °C for an additional 12 h. The reaction mixture was cooled to room temperature and added dropwise into methanol (100 mL) and the mixture was stirred for 1 h. Then the precipitated product was collected by filtration, and subjected to consecutive Soxhlet extractions with acetone, hexane and chloroform. The remaining solid was dissolved in hot TCE, then precipitated from methanol. Yield: 53 mg (53%). HT-GPC: M_n = 25.9 kDa; PDI = 2.7. Elemental anal. calcd for $(C_{112}H_{178}N_2O_6S_4)_n$: C, 75.71; H, 10.10; N, 1.58; found: C, 74.65; H, 10.42; N, 1.71.

Synthesis of PIDTOBTz. To a 25 mL dry Schlenk flask was added **IDTO-40** (50 mg, 0.028 mmol), 5,5′-bis(trimethylstannyl)-2,2′-bithiazole (14.23 mg, 0.029 mmol) and tri(*o*-tolyl)phosphine (0.68 mg, 8 mol%). After degassing and refilling argon for 3 times, a solution of tris(dibenzylideneacetone)-dipalladium (0.51 mg, 2 mol%) in dry chlorobenzene (3 mL) was added under an argon atmosphere. The flask was sealed and stirred for at 130 °C for 48 h. Four drops of bromobenzene was added and the reaction was kept at 130 °C for an additional 12 h. The reaction mixture was cooled to room temperature and added dropwise into methanol (100 mL) and the mixture was stirred for 1 h. Then the precipitated product was collected by filtration, and subjected to consecutive Soxhlet extractions with acetone, hexane and chloroform. The chloroform solution was precipitated from methanol. Yield: 45 mg (89%). HT-GPC: M_n = 14.3 kDa; PDI = 2.5. Elemental anal. calcd for $(C_{110}H_{176}N_4O_6S_4)_n$: C, 74.27; H, 9.97; N, 3.15; found: C, 72.94; H, 10.37; N, 3.49.

Results and discussion

Synthesis and thermal properties of the polymers

PIDTOBT and **PIDTOBTz** were synthesized *via* Stille-coupling polymerizations between **IDTO-40** and organotin monomers with the $Pd_2(dba)_3/P(o\text{-tolyl})_3$ catalyst system (Scheme 1). It should be mentioned that the freshly prepared 5,5′-bis(trimethylstannyl)-2,2′-bithiazole should be used to carry out

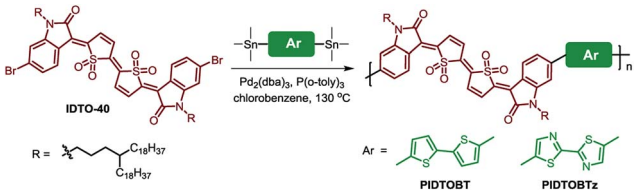

Scheme 1 Synthetic route to **PIDTOBT** and **PIDTOBTz** *via* Stille-coupling polymerization.

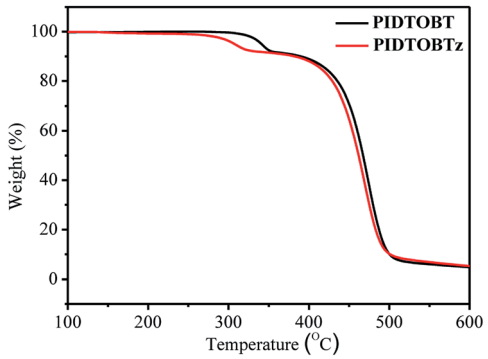

Fig. 1 TGA curves of **PIDTOBT** and **PIDTOBTz** at a heating rate of 10 °C min^{-1} under nitrogen.

the polymerization due to its limited stability.[40] **PIDTOBT** could only be dissolved in hot 1,1,2,2-tetrachloroethane (TCE), while **PIDTOBTz** showed much better solubility with 89% of it could be extracted with chloroform. Their different solubilities may be ascribed to their different molecular weights and interchain D–A interactions (*vide infra*). The number average molecular weight (M_n) and polydispersity index (PDI) were measured to be 25.9 kDa and 2.7 for **PIDTOBT** and 14.3 kDa and 2.5 for **PIDTOBTz**, determined by high-temperature gel-permeation chromatography (HT-GPC) at 140 °C using polystyrene as the standard. The unstable 5,5′-bis(trimethylstannyl)-2,2′-bithiazole might decompose during the polymerization, resulting in the lower molecular weight of **PIDTOBTz**. Both polymers are quite thermally stable with temperatures for 5% weight loss at 341 °C and 308 °C under nitrogen and at 315 °C and 282 °C in air (Fig. S6†) for **PIDTOBT** and **PIDTOBTz**, respectively. The first-step weight loss observed for the samples measured under nitrogen (Fig. 1) is considered due to the decomposition of the thiophene-*S*,*S*-dioxide units to release SO_2 because of the relatively labile C–S bonds.[25,41] No thermal transitions were observed from differential scanning calorimetry (DSC) measurements (Fig. S7†).

Theoretical calculation

We conducted a computational study by density functional theory (DFT) to investigate the geometry, molecular energy levels, and electron distributions of their model dimer compounds (Fig. 2). The HOMO wavefunctions of the two polymers are well delocalized along the polymer backbones, whereas the LUMO wavefunctions are mostly localized on the IDTO cores. The LUMO and HOMO energy levels of the **IDTOBT-Me** dimer were calculated to be −3.55 eV and −5.32 eV, respectively. The LUMO and HOMO energy levels of the **IDTOBTz-Me** dimer were calculated to be −3.67 eV and −5.64 eV, respectively, which are lower than those of the **IDTOBT-Me** dimer due to the more electron deficient nature of BTz. The IDTO building block is completely coplanar. The dihedral angles between the thiophene and IDTO in **IDTOBT-Me** and between thiazole and IDTO in **IDTOBTz-Me** are ∼20°, while those of the BT and BTz segments are 0.8° and ∼0°, respectively.

Photophysical and electrochemical properties

To reveal their absorption characteristics, **PIDTOBT** and **PIDTOBTz** were measured in dilute TCE solutions, showing the wavelengths of maximum absorption (λ_{max}) at 780 nm and 636

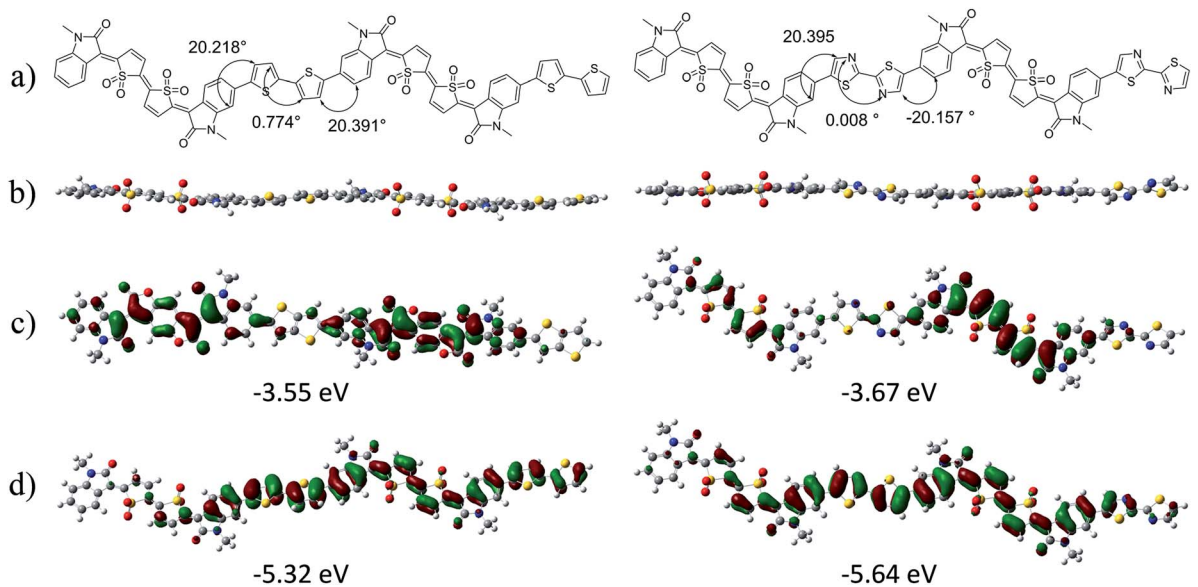

Fig. 2 (a) Structure, (b) geometries, (c) LUMO, and (d) HOMO of **IDTOBT-Me** and **IDTOBTz-Me** dimers optimized by computer simulations.

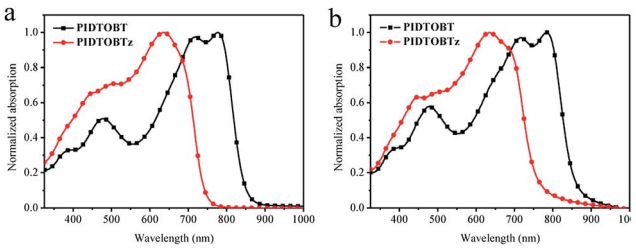

Fig. 3 UV-Vis-NIR absorption spectra of **PIDTOBT** and **PIDTOBTz** in TCE solution (a) and in thin films (b).

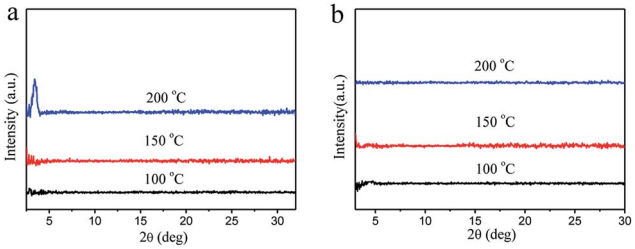

Fig. 5 XRD patterns of the polymer films on SiO_2/Si substrate at annealed different temperatures: (a) **PIDTOBT**; (b) **PIDTOBTz**.

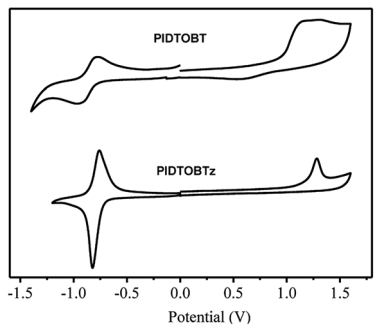

Fig. 4 Cyclic voltammograms of **PIDTOBT** and **PIDTOBTz** films measured in dry acetonitrile containing 0.1 M n-Bu_4NPF_6 as an electrolyte under nitrogen at a scan rate of 100 mV s^{-1}.

nm, respectively (Fig. 3a). The much longer λ_{max} for **PIDTOBT** with respect to **PIDTOBTz** most likely resulted from the stronger electron-donating property of the BT unit as compared to the BTz unit. Going from solution to the film state, no significant changes are observed in the absorption profiles of both polymers, indicating that there might be some pre-aggregation in solution. The same phenomenon was also observed for some other D–A polymers.[8,42,43] Based on the film absorption onsets, the optical band gaps (E_g^{opt}) of **PIDTOBT** and **PIDTOBTz** are estimated to be 1.43 eV and 1.62 eV, respectively.

The HOMO and LUMO levels of **PIDTOBT** and **PIDTOBTz** were measured by cyclic voltammetry (CV) (Fig. 4). Both polymers exhibit reversible reduction peaks, where **PIDTOBTz** showed a large reduction peak current and a more reversible reduction cycle than **PIDTOBT**. The LUMO and HOMO energy levels of **PIDTOBT** are −4.09 eV and −5.78 eV, obtained from the reduction and oxidation onset potentials in its CV diagram, respectively. **PIDTOBTz** exhibited deeper LUMO and HOMO energy levels of −4.18 and −5.99 eV, which is consistent with our DFT results. Compared to our previously reported polymer, **PIDTOTT** (LUMO = −3.98 eV; HOMO = −5.92 eV), both polymers in this study exhibited lower LUMO energy levels, suggesting their smaller electron injection barriers in OTFTs.

Microstructure of the thin films

The crystallinity of polymers was studied by using X-ray diffractometry (XRD) of polymer thin films spin coated on dodecyltrichlorosilane (DDTS) modified SiO_2/Si substrates. As shown in Fig. 5, for the 100 °C and 150 °C-annealed thin films, both polymers show no appreciable diffraction peaks. Once the annealing temperature was raised to 200 °C, a weak primary peak (100) at $2\theta = 3.4°$ (d-spacing = 2.59 nm) appeared for the **PIDTOBT** film, suggesting that some degree of chain ordering starts to form at that annealing temperature. Compared with the film of **PIDTOTT**, which presented a weak hump at the same position after annealing at 200 °C,[25] **PIDTOBT** film showed improved crystallinity. **PIDTOBTz** showed no reflection peaks at all annealing temperatures, indicating the poor molecular ordering in its thin films. The atomic force microscopy (AFM) height images of the films spin coated on DDTS-modified SiO_2/Si are shown in Fig. S8 and S9.† Small inter-connected grains are observed for the **PIDTOBT** thin film annealed at 100 °C. After annealing at 200 °C, the grains have grown notably, and the root mean squared roughness (R_q) increased from 2.7 nm to 4.3 nm. Larger grains could reduce the number of grain boundaries, thereby improving the charge transport. On the other hand, all the annealed **PIDTOBTz** thin films consist of much smaller grains, which is in agreement with their poor crystallinity verified by XRD analysis.

OTFT performance

PIDTOBT and **PIDTOBTz** were tested as channel semiconductors in bottom-gate, bottom-contact (BGBC) OTFTs. Heavily n-doped Si/SiO_2 wafer patterned with gold source and drain electrode pairs was used as the substrate. A polymer solution in TCE (**PIDTOBT**) or chloroform (**PIDTOBTz**) was spin coated on the substrate to form a polymer thin film (~40 nm), which was annealed at 100, 150, or 200 °C on a hot plate. The devices were tested in the nitrogen filled glove box. As shown in Fig. 6 and Table 1, both polymers exhibit typical n-channel charge transport characteristics. Devices with the 100 °C annealed **PIDTOBT** films exhibited an electron mobility of 0.069 cm^2 V^{-1} s^{-1}. For the 150 °C-annealed thin films, the maximum electron mobility significantly improved to 0.12 cm^2 V^{-1} s^{-1}. When the thin films were annealed at 200 °C, the devices gave the highest electron mobility of up to 0.18 cm^2 V^{-1} s^{-1} with a low threshold voltage of 2.3 V and a high current on/off ratio of ~10^5. The dependence of OTFT performances on the annealing temperature is in good agreement with the XRD results. These device data clearly show that **PIDTOBT** has better electron transport capability than **PIDTOTT**. This may be originated from the lower LUMO energy level and the higher crystallinity of **PIDTOBT**.

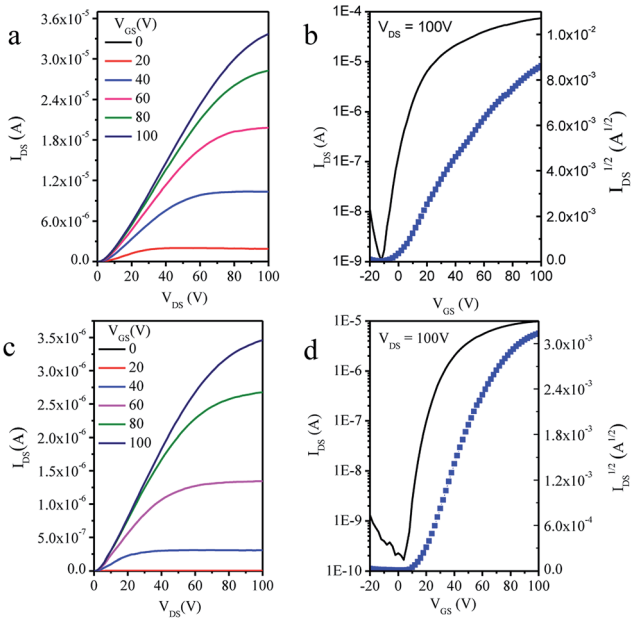

Fig. 6 Output (a and c) and transfer (b and d) curves of an OTFT device based on a thin film of **PIDTOBT** (a and b) and **PIDTOBTz** (c and d) annealed at 200 °C.

Table 1 OTFT performance of **PINDFTT** and **PINDFBT**

Polymer	Annealing temperature (°C)	Avg. ± std (max.) electron mobility ($cm^2 V^{-1} s^{-1}$)
PIDTOBT	100	0.060 ± 0.0091 (0.072)
	150	0.110 ± 0.0120 (0.125)
	200	0.140 ± 0.0153 (0.180)
PIDTOBTz	100	0.015 ± 0.0001 (0.016)
	150	0.016 ± 0.0015 (0.017)
	200	0.014 ± 0.0019 (0.016)

However, although **PIDTOBTz** has a lower LUMO energy level than **PIDTOBT**, the devices based on **PIDTOBTz** showed much lower performance with the highest electron mobility of 0.017 $cm^2 V^{-1} s^{-1}$ at an annealing temperature of 150 °C. The device performance of **PIDTOBTz** almost did not change with varying annealing temperature. The poor crystallinity and low molecular weight are considered responsible for the low mobility of **PIDTOBTz**. When the 200 °C-annealed devices were tested under ambient conditions without any encapsulation, the highest electron mobility of **PIDTOBT** decreased to 0.11 $cm^2 V^{-1} s^{-1}$. Whereas, **PIDTOBTz** showed better stability in air with the highest electron mobility of 0.013 $cm^2 V^{-1} s^{-1}$, which may be accounted for its deeper LUMO energy level. The dramatic differences in the device performance between **PIDTOBT** and **PIDTOBTz** suggest that the molecular weight and the crystallinity of the thin films have more significant impact on the charge transport performance, while the LUMO energy level of the polymer may play an important role in the device stability in air.

Conclusions

In summary, two novel IDTO-based low-bandgap donor–acceptor polymers, **PIDTOBT** and **PIDTOBTz**, with low LUMO energy levels have been developed for n-type OTFTs. **PIDTOBT** with BT units showed a lower LUMO energy level and higher crystallinity, and exhibited high electron mobility up to 0.18 $cm^2 V^{-1} s^{-1}$. **PIDTOBTz** with BTz units has a much lower LUMO energy level, but poorer crystallinity. **PIDTOBTz** exhibited a one order of magnitude lower electron mobility of 0.017 $cm^2 V^{-1} s^{-1}$, which is accounted for its poor crystallinity and lower molecular weight. The electron mobilities of **PIDTOBT** are comparable to those (0.1–0.3 $cm^2 V^{-1} s^{-1}$) of the reported high performance n-type polymers that were evaluated with the same BGBC device configuration on SiO_2/Si substrates.[44–46] Significantly higher mobility values were achieved for several high performance n-type polymers[44–47] when a top-gate bottom-contact (TGBC) device configuration was adopted since charge traps on the SiO_2 dielectric surface[48] and contact resistance[49] can be effectively reduced compared to the BGBC devices. Higher mobility is expected if the crystallinity of IDTO polymers can be further improved by incorporating other types of co-monomer building blocks and/or side chain engineering and by optimizing device fabrication.

Acknowledgements

The authors thank the Natural Sciences and Engineering Research Council (NSERC) of Canada for the financial support (Discovery Grants #402566-2011) of this work.

References

1 H. Yan, Z. Chen, Y. Zheng, C. Newman, J. R. Quinn, F. Dotz, M. Kastler and A. Facchetti, *Nature*, 2009, **457**, 679–686.
2 S. C. B. Mannsfeld, B. C.-K. Tee, R. M. Stoltenberg, C. V. H.-H. Chen, S. Barman, B. V. O. Muir, A. N. Sokolov, C. Reese and Z. Bao, *Nat. Mater.*, 2010, **9**, 859–864.
3 J. Mei, Y. Diao, A. L. Appleton, L. Fang and Z. Bao, *J. Am. Chem. Soc.*, 2013, **135**, 6724–6746.
4 J. F. Martínez Hardigree and H. E. Katz, *Acc. Chem. Res.*, 2014, **47**, 1369–1377.
5 J. Li, Y. Zhao, H. S. Tan, Y. Guo, C.-A. Di, G. Yu, Y. Liu, M. Lin, S. H. Lim, Y. Zhou, H. Su and B. S. Ong, *Sci. Rep.*, 2012, **2**, 754.
6 I. Kang, H.-J. Yun, D. S. Chung, S.-K. Kwon and Y.-H. Kim, *J. Am. Chem. Soc.*, 2013, **135**, 14896–14899.
7 G. Kim, S.-J. Kang, G. K. Dutta, Y.-K. Han, T. J. Shin, Y.-Y. Noh and C. Yang, *J. Am. Chem. Soc.*, 2014, **136**, 9477–9483.
8 Z. Zhao, F. Zhang, Y. Hu, Z. Wang, B. Leng, X. Gao, C. Di and D. Zhu, *ACS Macro Lett.*, 2014, **3**, 1174–1177.
9 T. Lei, X. Xia, J.-Y. Wang, C.-J. Liu and J. Pei, *J. Am. Chem. Soc.*, 2014, **136**, 2135–2141.
10 J. Zaumseil and H. Sirringhaus, *Chem. Rev.*, 2007, **107**, 1296–1323.
11 K.-J. Baeg, M. Caironi and Y.-Y. Noh, *Adv. Mater.*, 2013, **25**, 4210–4244.

12 B. Sun, W. Hong, Z. Yan, H. Aziz and Y. Li, *Adv. Mater.*, 2014, **26**, 2636–2642.
13 Y. He, W. Hong and Y. Li, *J. Mater. Chem. C*, 2014, **2**, 8651–8661.
14 H. Usta, C. Risko, Z. Wang, H. Huang, M. K. Deliomeroglu, A. Zhukhovitskiy, A. Facchetti and T. J. Marks, *J. Am. Chem. Soc.*, 2009, **131**, 5586–5608.
15 Q. Wu, R. Li, W. Hong, H. Li, X. Gao and D. Zhu, *Chem. Mater.*, 2011, **23**, 3138–3140.
16 W. Hong, C. Guo, B. Sun, Z. Yan, C. Huang, Y. Hu, Y. Zheng, A. Facchetti and Y. Li, *J. Mater. Chem. C*, 2013, **1**, 5624–5627.
17 T. Lei, J.-H. Dou, X.-Y. Cao, J.-Y. Wang and J. Pei, *J. Am. Chem. Soc.*, 2013, **135**, 12168–12171.
18 Z. Yan, B. Sun and Y. Li, *Chem. Commun.*, 2013, **49**, 3790–3792.
19 A. J. Tilley, C. Guo, M. B. Miltenburg, T. B. Schon, H. Yan, Y. Li and D. S. Seferos, *Adv. Funct. Mater.*, 2015, **25**, 3321–3329.
20 T. Lei, J.-H. Dou, X.-Y. Cao, J.-Y. Wang and J. Pei, *Adv. Mater.*, 2013, **25**, 6589–6593.
21 S. Subramaniyan, T. Earmme, N. M. Murari and S. A. Jenekhe, *Polym. Chem.*, 2014, **5**, 5707–5715.
22 C. Wang, H. Dong, W. Hu, Y. Liu and D. Zhu, *Chem. Rev.*, 2012, **112**, 2208–2267.
23 H. Li, F. S. Kim, G. Ren and S. A. Jenekhe, *J. Am. Chem. Soc.*, 2013, **135**, 14920–14923.
24 Y. Zhao, Y. Guo and Y. Liu, *Adv. Mater.*, 2013, **25**, 5372–5391.
25 Y. Deng, B. Sun, Y. He, J. Quinn, C. Guo and Y. Li, *Angew. Chem., Int. Ed.*, 2016, **55**, 3459–3462.
26 J. D. Yuen and F. Wudl, *Energy Environ. Sci.*, 2013, **6**, 392–406.
27 D. E. Janzen, M. W. Burand, P. C. Ewbank, T. M. Pappenfus, H. Higuchi, D. A. da Silva Filho, V. G. Young, J.-L. Brédas and K. R. Mann, *J. Am. Chem. Soc.*, 2004, **126**, 15295–15308.
28 H. Hwang, D. Khim, J.-M. Yun, E. Jung, S.-Y. Jang, Y. H. Jang, Y.-Y. Noh and D.-Y. Kim, *Adv. Funct. Mater.*, 2015, **25**, 1146–1156.
29 J. L. Brédas, B. Thémans, J. G. Fripiat, J. M. André and R. R. Chance, *Phys. Rev. B: Condens. Matter Mater. Phys.*, 1984, **29**, 6761–6773.
30 J. L. Bredas and G. B. Street, *Acc. Chem. Res.*, 1985, **18**, 309–315.
31 J. Roncali, *Chem. Rev.*, 1997, **97**, 173–206.
32 X. Guo, R. P. Ortiz, Y. Zheng, Y. Hu, Y.-Y. Noh, K.-J. Baeg, A. Facchetti and T. J. Marks, *J. Am. Chem. Soc.*, 2011, **133**, 1405–1418.
33 X. Guo, R. P. Ortiz, Y. Zheng, M.-G. Kim, S. Zhang, Y. Hu, G. Lu, A. Facchetti and T. J. Marks, *J. Am. Chem. Soc.*, 2011, **133**, 13685–13697.
34 Y. Li, P. Sonar, S. P. Singh, M. S. Soh, M. van Meurs and J. Tan, *J. Am. Chem. Soc.*, 2011, **133**, 2198–2204.
35 T. Lei, Y. Cao, Y. Fan, C.-J. Liu, S.-C. Yuan and J. Pei, *J. Am. Chem. Soc.*, 2011, **133**, 6099–6101.
36 J. Liu, R. Zhang, I. Osaka, S. Mishra, A. E. Javier, D.-M. Smilgies, T. Kowalewski and R. D. McCullough, *Adv. Funct. Mater.*, 2009, **19**, 3427–3434.
37 D. H. Kim, B.-L. Lee, H. Moon, H. M. Kang, E. J. Jeong, J.-I. Park, K.-M. Han, S. Lee, B. W. Yoo, B. W. Koo, J. Y. Kim, W. H. Lee, K. Cho, H. A. Becerril and Z. Bao, *J. Am. Chem. Soc.*, 2009, **131**, 6124–6132.
38 Y. Lin, H. Fan, Y. Li and X. Zhan, *Adv. Mater.*, 2012, **24**, 3087–3106.
39 J. Lee, J. W. Chung, J. Jang, D. H. Kim, J.-I. Park, E. Lee, B.-L. Lee, J.-Y. Kim, J. Y. Jung, J. S. Park, B. Koo, Y. W. Jin and D. H. Kim, *Chem. Mater.*, 2013, **25**, 1927–1934.
40 B. Fu, C.-Y. Wang, B. D. Rose, Y. Jiang, M. Chang, P.-H. Chu, Z. Yuan, C. Fuentes-Hernandez, B. Kippelen, J.-L. Brédas, D. M. Collard and E. Reichmanis, *Chem. Mater.*, 2015, **27**, 2928–2937.
41 C. Zhang, T. H. Nguyen, J. Sun, R. Li, S. Black, C. E. Bonner and S.-S. Sun, *Macromolecules*, 2009, **42**, 663–670.
42 N. Zhou, X. Guo, R. P. Ortiz, S. Li, S. Zhang, R. P. H. Chang, A. Facchetti and T. J. Marks, *Adv. Mater.*, 2012, **24**, 2242–2248.
43 X. Zhou, N. Ai, Z.-H. Guo, F.-D. Zhuang, Y.-S. Jiang, J.-Y. Wang and J. Pei, *Chem. Mater.*, 2015, **27**, 1815–1820.
44 H. Yan, Z. Chen, Y. Zheng, C. Newman, J. R. Quinn, F. Dötz, M. Kastler and A. Facchetti, *Nature*, 2009, **457**, 679–686.
45 T. Lei, J.-H. Dou, X.-Y. Cao, J.-Y. Wang and J. Pei, *Adv. Mater.*, 2013, **25**, 6589–6593.
46 H. Li, F. S. Kim, G. Ren and S. A. Jenekhe, *J. Am. Chem. Soc.*, 2013, **135**, 14920–14923.
47 C. Kanimozhi, N. Yaacobi-Gross, K. W. Chou, A. Amassian, T. D. Anthopoulos and S. Patil, *J. Am. Chem. Soc.*, 2012, **134**, 16532–16535.
48 R. P. Ortiz, A. Facchetti and T. J. Marks, *Chem. Rev.*, 2010, **110**, 205–239.
49 C. Di, Y. Liu, G. Yu and D. Zhu, *Acc. Chem. Res.*, 2009, **42**, 1573–1583.

